



Historical Biology

An International Journal of Paleobiology



ISSN: (Print) (Online) Journal homepage: <https://www.tandfonline.com/loi/ghbi20>

Brain endocast of two non-mammaliaform cynodonts from southern Brazil: an ontogenetic and evolutionary approach

Carolina A. Hoffmann, P. G. Rodrigues, M. B. Soares & M. B. Andrade

To cite this article: Carolina A. Hoffmann, P. G. Rodrigues, M. B. Soares & M. B. Andrade (2021) Brain endocast of two non-mammaliaform cynodonts from southern Brazil: an ontogenetic and evolutionary approach, *Historical Biology*, 33:8, 1196-1207, DOI: [10.1080/08912963.2019.1685512](https://doi.org/10.1080/08912963.2019.1685512)

To link to this article: <https://doi.org/10.1080/08912963.2019.1685512>




View supplementary material 



Published online: 01 Nov 2019.




Submit your article to this journal 



Article views: 175



View related articles 



View Crossmark data 



Citing articles: 2 View citing articles 

ARTICLE



Brain endocast of two non-mammaliaform cynodonts from southern Brazil: an ontogenetic and evolutionary approach

Carolina A. Hoffmann^a, P. G. Rodrigues^b, M. B. Soares^{b*} and M. B. de Andrade^{a,c}

^aEscola de Ciências da Saúde e da Vida, PUCRS, Pontifícia Universidade Católica do Rio Grande do Sul, Porto Alegre, Brasil; ^bInstituto de Geociências, Departamento de Paleontologia e Estratigrafia, Universidade Federal do Rio Grande do Sul, Porto Alegre, Brasil; ^cMuseu de Ciências e Tecnologia, PUCRS, Pontifícia Universidade Católica do Rio Grande do Sul, Porto Alegre, Brasil

ABSTRACT

Computed tomography is a non-destructive method that facilitates the accurate analysis of the internal structures of fossils. Several paleoneurological studies concerning derived non-mammaliaform cynodonts, mammaliaforms and basal mammals using this technique have been published. However, little remains known regarding the brain anatomy of basal Cynodontia. Thus, it is relevant to increase knowledge concerning the basal members of this clade to obtain a better understanding of brain evolution during the descent of mammals from non-mammaliaform cynodonts. Therefore, the present study involved analysing the digital endocasts of two non-mammaliaform cynodonts (*Probelesodon kitchingi* and *Massetognathus ochagaviae*). To assess the rate of brain development, the encephalisation quotients for these species were calculated and compared with previous data. Compared to a previous study on the brain endocasts of *Probelesodon* sp. and *Massetognathus* sp. from Argentina, digital endocasts of the Brazilian specimens revealed new brain morphology features for these genera. Additionally, the 3D digital endocasts and EQ estimates are relevant for assessing intraspecific variation and possible ontogenetic changes in these fossil taxa.

ARTICLE HISTORY

Received 15 July 2019
Accepted 23 October 2019

KEYWORDS

Brain evolution; cynodontia; encephalization quotient; triassic

Introduction

The evolution of the brain can be studied through casts of the cranial cavities of extinct vertebrate species (e.g. Jerison 1973). These paleoneurological studies are limited to external and indirect analysis based on cranial endocasts, which can be exposed naturally, or by fossil preparation (Hopson 1979) and, more recently, through digital visualisation using computed tomography (CT-scan) (e.g. Macrini et al. 2006, 2007; Rowe et al. 2011). An endocast can provide the general shape and volume of the brain of a given animal in life, which can be useful for functional or palaeoecological inference, as well as for understanding the locomotor or feeding habits and behaviour (e.g. Napoli et al. 2017; Bronzati et al. 2017; Benoit et al. 2015, 2017b). The evolution of improving the capacity to process information can be addressed through the degree of encephalisation (increase in relative brain size; Jerison 1985). The equation developed by Jerison (1973), known as the Encephalization Quotient (EQ), represents the brain development for a certain taxon relative to the volume expected for a reference taxon (of the same size and age) and provides quantitative data on brain evolution. It is the most commonly used method in encephalisation analysis, including basal cynodonts and mammals (e.g. Quiroga 1979, 1980, 1984; Kielan-Jaworowska and Lancaster 2004; Macrini et al. 2006).


More recently, CT-scan techniques, such as micro-CT (Abel et al. 2012) and synchrotron scanning (Tafforeau et al. 2006), are being applied to palaeontological research. These techniques represent non-destructive methods that permit the investigation of fossils' internal and external structures in high-quality three-dimensional images and incredible detail (Cnudde and Boone 2013;

Cunningham et al. 2014). As such, several paleoneurological studies concerning derived non-mammaliaform cynodonts, mammaliaforms and basal mammals using CT scanning techniques have been published (e.g. Macrini et al. 2006, 2007; Rowe et al. 2011; Rodrigues et al. 2014, 2018). In addition, recent endocast analyses of basal therapsids are revealing a morphological diversity of neurological structures of therapsid-mammal evolution (Castaninha et al. 2013; Laaß 2015; Laaß et al. 2017; Benoit et al. 2017a, 2017b), highlighting the importance of studying the endocasts of basal synapsids to improve our understanding of brain evolution in synapsids and mammals. However, the sample poorly reflects the diversity of synapsids from the Permian and Triassic, while little remains known regarding the brains of these taxa. Moreover, one specimen per taxon is typically used in non-mammaliaform cynodont endocast analysis; thus, the ontogenetic stage has not yet been discussed among Cynodontia paleoneurological studies. As a result, Quiroga (1979) noted the significance of contemplating the ontogenetic stage of fossils under study, as young specimens generally show a greater relative brain size and variation in the relative proportions of different brain regions, which can subsequently influence EQ values and the interpretation of results.

In the present study, we present the description of digitally reconstructed cranial endocasts of two non-mammaliaform cynodont specimens (MCP 3871 PV *Massetognathus ochagaviae* Barberena 1981 – neotype; and MCP 1600 PV *Probelesodon kitchingi*; Sá-Teixeira 1982 – holotype) based on CT-scan images. The results are compared with previous paleoneurological analyses of specimens of the same genus based on natural endocasts (Quiroga 1979) and other non-mammalian cynodonts to discuss the

CONTACT Carolina A. Hoffmann  carolina.hoffmann@acad.pucrs.br

*Present address: Departamento de Geologia e Paleontologia, Museu Nacional/UFRJ, Universidade Federal do Rio de Janeiro, Parque Quinta da Boa Vista, Mangueira, CEP 20940040, Rio de Janeiro, Brasil. E-mail: marina.soares@mn.ufrj.br

 Supplemental data for this article can be accessed [here](#).

© 2019 Informa UK Limited, trading as Taylor & Francis Group

implications of EQ values and potential inferences related to ontogenetic stage in these studies.

Previously described morphological traits of non-mammaliaform cynodont endocasts

Endocast descriptions have been published for a few basal Cynodontia taxa: the Early Triassic *Thrinaxodon liorhinus*, *Diademodon*, and *Trirachodon*; the Late Permian *Procynosuchus*; the Middle Triassic *Massetognathus*, *Probelesodon*, *Probainognathus* and *Chiniquodon theotonicus* and the Late Triassic *Exaeretodon argentinus*, *E. riograndensis*, *Therioherpeton carnini*, *Brasilitherium riograndensis* and *Riograndia guaibensis* (Watson 1913; Bonaparte 1966; Hopson 1979; Kemp 1979, 2009; Quiroga 1979, 1980, 1984; Rodrigues et al. 2014, 2018; Pavanatto et al. 2019). These previous works showed that the non-mammaliaform cynodonts endocast is generally anteroposteriorly elongated with a tubular shape telencephalon, and in most species, the cerebral hemispheres are not separated and expanded. The widest region is represented by the prominent and laterally expanded *paraflocculi* lobes, a cerebellar region. In most non-mammaliaform cynodonts the floor of the frontal part of the braincase was presumably formed by the cartilaginous structures of the chondrocranium; therefore, the lack of ossification in this region hinders the accurate visualisation of the ventral limits of the forebrain endocast (Rowe et al. 1994; Kielan-Jaworowska et al. 2004). However, a partially ossified orbitosphenoid floor is present in the chiniquodontids *Probelesodon* sp. and *C. theotonicus* (Quiroga 1979; Kemp 2009) and the 'gomphodonts' *Trirachodon* sp., *Massetognathus* sp. and *E. riograndensis* (Hopson 1979; Quiroga 1979; Pavanatto et al. 2019); therefore, the endocast ventral limit can be better observed in these taxa, resulting in more reliable data.

The main visible structure of the forebrain is the well-marked cast of olfactory bulbs, that gradually contacts the cerebral hemispheres, though the limits between them are not well-marked on endocasts (Jerison 1973; Hopson 1979), even though olfactory peduncles are present in *Massetognathus* sp and *Probainognathus* (Quiroga 1979, 1980). The parietal foramen and corresponding pineal body on the dorsal surface of the endocast are present in some taxa, while the absence of a parietal foramen is a derived feature for Cynodontia (Kielan-Jaworowska et al. 2004). Another usual feature is the presence of a hypophyseal cast on the ventral region, which fills the *sella turcica* on the basisphenoid/parasphenoid complex (Rodrigues et al. 2018).

The midbrain region may not be exposed in endocasts because it is covered by meninges and blood sinuses or due to the presence of the telencephalon being posteriorly expanded or an anteriorly expanded cerebellum (Edinger 1964). Regarding cynodonts, the portion of the midbrain that may be exposed on the dorsal surface of the endocast corresponds mainly to the anterior and posterior *colliculi*. The dorsal exposure of the midbrain was described for *Probainognathus* and *Therioherpeton* (Quiroga 1980, 1984). However, Kielan-Jaworowska et al. (2004) argued that this structure could be the result of post-mortem changes in parts of the brain and meninges. Therefore, the exposure of the dorsal midbrain in the endocast of non-mammaliaform cynodonts remains controversial and its non-exposure may thus represent the apomorphic condition of extant mammals (see Macrini et al. 2007).

The interpretation and description of the endocast structures comprising the hindbrain may be difficult due to the poor ossification of this skull region in some basal therapsids and non-mammaliaform cynodonts (Kielan-Jaworowska et al. 2004). Nevertheless, the parafloccular region is usually described for brain endocasts, which fill the subarcuate fossa on the supraoccipital and the petiotic components of the skull (Kemp 2009). This

cerebellar region is largely responsible for body coordination, balance and the coordination of eye movements; therefore, enlarged *paraflocculi* could indicate well-developed visual and locomotor capabilities (Butler and Hodos 2005). Kielan-Jaworowska et al. (2004) indicated the presence of the cerebellar vermis on the posterior region of a *Thrinaxodon* endocast; however, other authors considered this protuberance an artefact of the filling of a cartilaginous space in the supraoccipital (e.g. Quiroga 1979) or superior sagittal sinus (Rowe et al. 1994; Kemp 2009).

Previous descriptions of non-mammalian synapsids brain cavities revealed the presence of a mid-dorsal depression enclosed by the parietal, interparietal and supraoccipital bones (Laaß et al. 2017). Known as the 'unossified zone', this region was described as the filling of the cartilaginous region by some authors, although it was also suggested to house the vermis, the superior sagittal sinus, a junction of several blood vessels, the pineal gland or other mid-brain structures; therefore, the function of this skull region remains unknown (Laaß et al. 2017).

Materials and methods

The specimens used in this study were collected in Triassic outcrops on the central region of Rio Grande do Sul state, southern Brazil, corresponding to the Santa Maria Supersequence (SMS; Figure 1). According to Zeffass et al. (2003), this geological setting is composed of three third-order sequences: (1) Santa Maria Sequence I (SMSI), which comprises conglomerates and cross-bedded sandstones, that are overlaid by laminated mudstones and interpreted as fluvial deposits transitioning into shallow lacustrine deposits. Posteriorly, Horn et al. (2014) subdivided the SMSI into the Pinheiros-Chiniquá and Santa Cruz Sequences; (2) Santa Maria Sequence II (SMSII), currently corresponding to the Candelária Sequence (Horn et al. 2014), is composed of medium-to fine-grained, cross-bedded sandstone and mudstone lenses at the base, grading to thick mudstones in the middle part, which are interpreted as high-sinuosity fluvial and overbank deposits, while the top portion of SMSII displays a coarsening-upward succession composed of rhythmites (siltstone-mudstone) intercalated with lenses of fine-grained, cross-bedded or cross-laminated sandstones, deposited in a lacustrine-deltaic system; and (3) Santa Maria Sequence III (SMSIII), which consists of cross-stratified, conglomeratic sandstones with abundant silicified logs. Lithostratigraphically, SMS I and II correspond to the Santa Maria and Caturrita Formations, while SMSIII corresponds to the Mata Formation (Zeffass et al. 2003).

As a sequence of geological units, these strata represent the progression of Triassic lacustrine/fluvial palaeoenvironments to dryer conditions culminating in desertic conditions, as evidenced by the aeolic deposits of the overlying Botucatu Formation (Scherer 2000; Pierini et al. 2002). Based on the correlation with Argentinian fossils, four faunal associations for Middle-Upper Triassic outcrops from southern Brazil were established in recent years (Horn et al. 2014; Marsicano et al. 2016). The *Dinodontosaurus* Assemblage Zone (AZ; Lower Carnian, Pinheiros-Chiniquá Sequence) is correlated with the tetrapod faunas of the Chañares Formation; the *Santacruzodon* AZ (Lower-Upper Carnian, Santa Cruz Sequence) is related to the basal layers of the Ischigualasto Formation and upper layers of the underlying Chañares Formation; the *Hyperodapedon* AZ (Carnian, Candelária Sequence) is correlated with Ischigualasto Formation; and the *Riograndia* AZ (Norian, Candelária Sequence) is associated with the lower fauna of the Los Colorados Formation (Soares et al. 2011; Horn et al. 2014; Martinelli et al. 2017). The non-mammaliaform cynodonts specimens analysed in this study corresponds to outcrops within the *Dinodontosaurus* AZ.

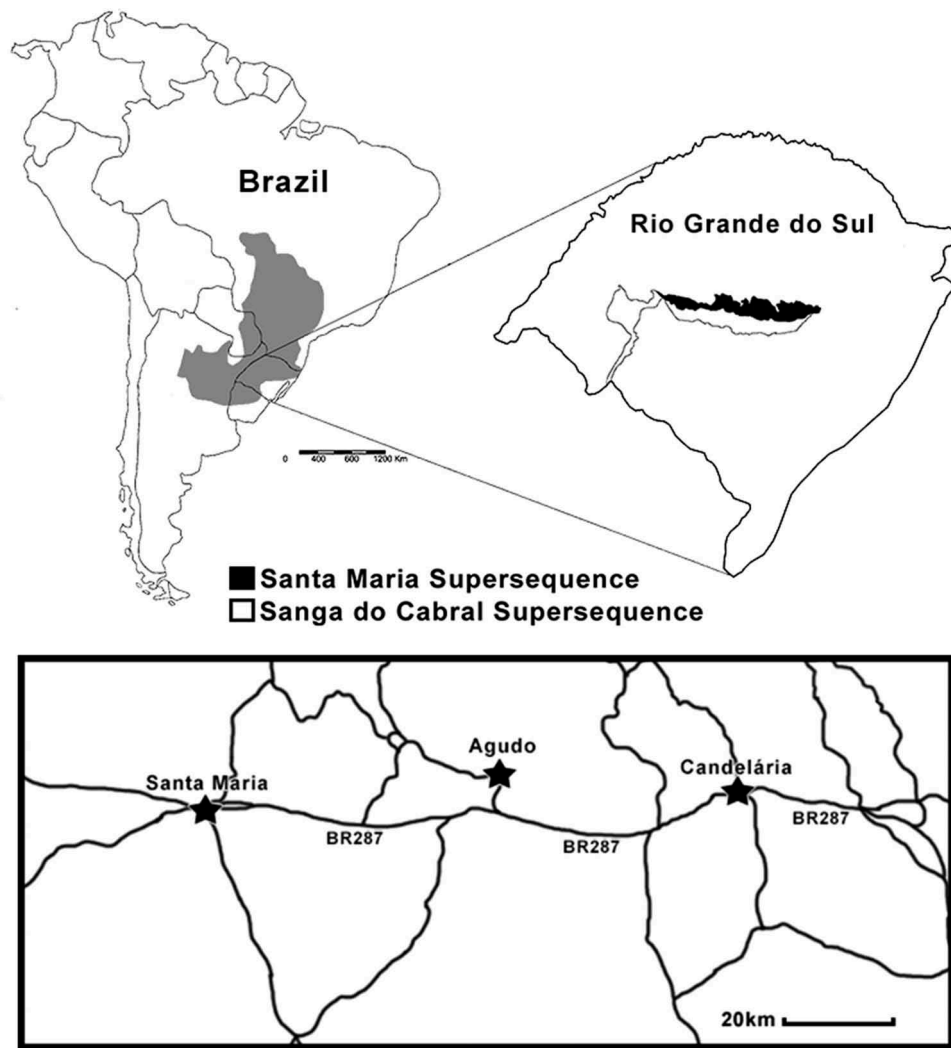


Figure 1. Locality of the specimens (MCP 1600 PV *Probelesodon kitchingi* and MCP 3871 PV *Massetognathus ochagaviae*) used in this study. The stars represent the cities near the outcrops where the fossils were found.

Analysed specimens

The studied specimens belong to the Paleovertebrate Fossil Collection (MCP-PV) of the Museu de Ciência e Tecnologia, Pontifícia Universidade Católica do Rio Grande do Sul (MCT-PUCRS), in Porto Alegre, Rio Grande do Sul state, Brazil. The precise outcrop location of the specimens was not provided by the collectors (see Barberena 1981; Sá-Teixeira 1982). Nonetheless, MCP 3871 PV *Massetognathus ochagaviae* (neotype; Figure 2) was collected near the city of Candelária, while MCP 1600 PV *Probelesodon kitchingi* (holotype; Figure 2) was collected in Rincão do Pinhal, Agudo municipality (Figure 1) both within the *Dinodontosaurus* AZ (Santa Maria Supersequence, Pinheiros-Chiniquá Sequence, Middle Triassic, Ladinian; Soares et al. 2011; Horn et al. 2014).

Notably, the specimen MCP 3871 PV is a well-preserved cranium (Figure 2). Despite breakage of the sagittal crest next to the interparietal contact, there is no damage to the endocranium. A portion of the prootic is broken and part of the epipterygoid is missing on the right side of the specimen. Moreover, the inner ear and quadrate are not preserved. Originally, the specimen UFRGS 0255 PV (a nearly complete skull) was described by Barberena (1981) as the

holotype of *M. ochagaviae*. However, it was lost in the 1990s. Hence, MCP 3871 PV is considered the neotype (Liu et al. 2008).

MCP 1600 PV is the holotype of *Probelesodon kitchingi* and comprises a cranium that is slightly distorted to the right from the original sagittal axis, particularly on the left temporal fenestra (Figure 2). Furthermore, a major portion of the left epipterygoid and prootic are broken, thus making it difficult to segment the endocranium in this region of the skull. Part of the basisphenoid, next to the contact with pterygoids on the left side, is also broken. Recently, *P. kitchingi* was designated as a junior synonym of *Chiniquodon theotonicus* (Abdala and Giannini 2002). However, with the description of specimens of *Aleodon cromptoni* from Brazil and its inclusion in Chiniquodontidae, a question about the monospecificity of the genus *Chiniquodon* was raised, resulted in this genus currently being interpreted as a 'waste-basket' group (see 'Discussion', below). Additionally, Martinelli et al. (2017) cited the presence of *A. cromptoni* specimens in the Brazilian sample analysed by Abdala and Giannini (2002), who referred to it as *C. theotonicus*, thereby highlighting the need for a family revision. Since *Chiniquodon* may currently represent a 'waste-basket' taxon, we prefer to address this specimen through its original status. Future alpha-taxonomic studies, which are outside the scope of this paper, may shed light on this subject.

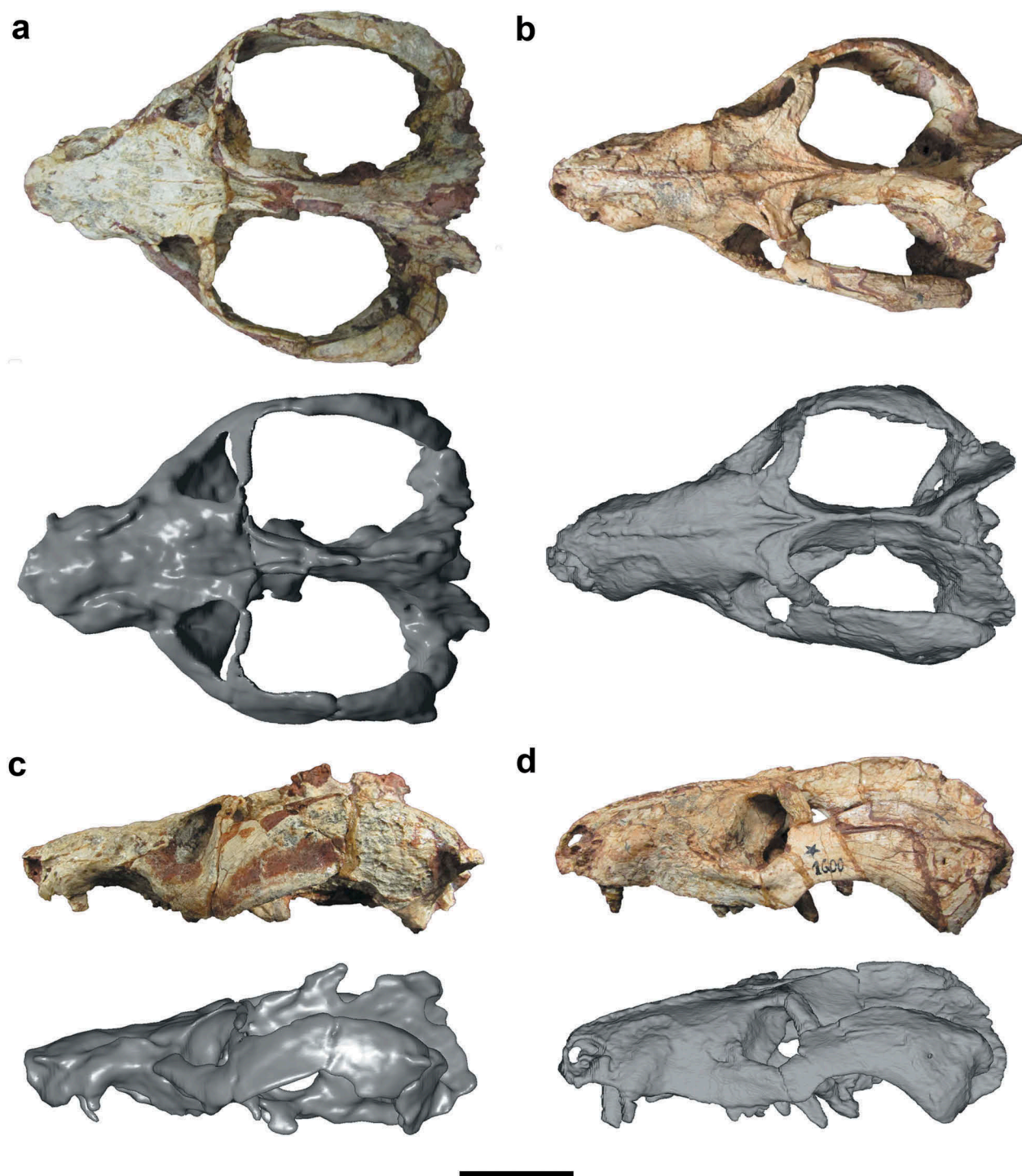


Figure 2. Photography (top) and 3D reconstructions (bottom) of *Massetognathus ochagaviae* (MCP 3871 PV, neotype) and *Probelesodon kitchingi* (MCP 1600 PV, holotype). (a, c), MCP 3871 PV in dorsal and lateral views; (b, d), MCP 1600 PV in dorsal and lateral views. All images are on the same scale. Scale bar: 50 mm.

Computed tomography

The CT-scan images were obtained using a medical CT scanner (Pet CT Multislice 16d Discovery) located at the Instituto do Cérebro facility, São Lucas Hospital. As a result of the CT scans, we obtained 676 slices of both skulls in transversal, coronal and sagittal planes, with a resolution of 512×512 pixels, 0.625 mm slices, 140kV and 380mA. The Triassic outcrops, where the materials used in the present study were collected, usually contain calcite in the rock matrix. This mineral interacts with X-rays, resulting in artefacts

on CT-scan images, which make it difficult to accurately visualise the fossil specimen and its internal structures (Cnudde and Boone 2013). We applied four protocols in an attempt to mitigate possible artefacts generated by the interaction of X-rays with calcite: default, soft, bone, and axial cut. As reported by Hoffmann et al. (2017), the soft protocol provided images of higher quality. This protocol operates with less focused X-ray beams and intensity, resulting in lower interaction with calcite and fewer artefacts. In addition, the soft protocol generated a better distinction between the rock matrix

and bone material density differences in comparison to the other protocols used. Therefore, the CT data used in this study was derived from this protocol.

Visualisation of the CT-scan slices, 3D models and segmentation of the brain endocast were performed using the software Avizo (version 7.1). The gray values of the images were altered to better visualise the density difference between the rock matrix and bony elements. The brain endocast was reconstructed by manually filling the corresponding cranial cavity in coronal view. The 3D digital brain endocasts and skull surfaces were analysed, edited and rendered with the open-source software MorphoDig (version 1.4; Lebrun 2018).

Quantitative analysis

Since the endocranial volume cannot be directly compared between species of different body mass, the EQ is used instead. The EQ is the ratio between the endocast volume (EV) observed for a given fossil taxon and the expected volume of the endocast for a specimen of the same body mass from a reference group (EV_r); this EV_r value is estimated through the use of the body mass (Jerison 1973). Body mass (BM, in grams) is calculated based in the skull length of the taxon, an equation provided for non-mammaliaform cynodonts by Quiroga (1979, 1980). The EV_r is therefore defined based on a reference group that, for cynodonts, is the volume expected for the endocast of an adult extant mammal with corresponding body size.

BM estimation is key for the proper calculation of EQ. BM estimation uses skull length to derive the mass, but this may vary for different skull:body proportions. Considering this, two equations (Equations 1 and 2) were used based on the relationship between skull length (S, in centimeters) and body weight in Therapsida (Quiroga 1979, 1980). Equation (2) is usually applied for 'heavy habitus' animals (Jerison 1973; Quiroga 1980); Equation (1) (herein referred as 'gracile habitus', in opposition) is used otherwise.

$$BM = 1,6S^3 \quad (1)$$

$$BM = 2,7S^3 \quad (2)$$

The specimens (MCP 3871 PV and MCP 1600 PV) were not associated with postcranial material, therefore the body masses (BM, in grams) of both specimens had to be estimated. It is assumed that BM estimation based on skull length is the same for cynodonts and extant mammals. This assumption is a common practice in the study of cynodont endocasts (Benoit et al 2017; Rodrigues et al. 2014, 2018). With effect, the description of complete body fossils of *Thrinaxodon*, *Galesaurus planiceps* and *Trucidocynodon riograndensis* suggests, that non-mammalian cynodonts and mammals had similar skull length:body mass relations (de Oliveira and Schultz 2016; Butler et al. 2019). However, the 'heavy habitus' equation is commonly used for most non-mammaliaform cynodonts (Jerison 1973; Quiroga 1980).

The EQs were calculated with two different equations (SI file), from the endocast volume (EV) and estimated BM. Equation 3 (Jerison 1973) is the most commonly used in the literature. Equation 4 (Manger 2006) is derived from Eisenberg EQ (1981) and is considered to be more mathematically accurate since it excludes outliers (as cetaceans and primates) from the regression equation calculation. In each equation we calculated four EQs (SI file): based on two endocast volumes, one with and one without the olfactory bulbs volume; and one for each body mass estimation (Equations 1 and 2). For comparative purposes, the EQ of other

Cynodontia taxa were also calculated when the necessary data were available (SI file).

$$EQ = EV / (0,12BM^{0,66}) \quad (3)$$

$$EQ = EV / (0,055BM^{0,7294}) \quad (4)$$

Absolute measurements of the total endocast length (TL), olfactory bulbs (OB), telencephalon (T) and hindbrain (HB) sizes were obtained through the ruler function the Avizo software. The endocast TL was measured from the anterior limit of the olfactory bulbs to the foramen magnum. OB length was measured from the anterior limit of the endocasts to posterior region of olfactory peduncles, represented by the narrowest section of the of the brain, located at the same relative position as the dorsal edge of the interorbital vacuity begins to curve towards the posterior wall of the vacuity. T length was measured from the end of the olfactory bulbs to the posterior limit of the base of the non-ossified region. HB length was measured from the posterior limit of the telencephalon to the foramen magnum. The OB, T and HB values were then scored against the total length of the endocast (TL) to produce relative measurements used for comparison with other taxa. As Quiroga (1979) provided no absolute values for *Massetognathus* and *Probelesodon*, we derived relative measurements from the available data (see Tables 1 and 2). We understand that these relative values are only the best possible approximation for comparison in the absence of absolute values.

Institutional abbreviations. MCP-PUCRS, Museu de Ciência e Tecnologia da PUCRS, Porto Alegre, Brazil; PVL, Instituto Miguel Lillo, Tucumán, Argentina.

Abbreviations in figures: cn, cranial nerve; F, frontal; FB, forebrain; fj, foramen jugular; fm, foramen magnum; fo, fenestra oval; HB, hindbrain; hf, hypophyseal fossa; hgf, hypoglossal foramen; iv, interorbital vacuity; MB, midbrain; mo, medula oblonga; op,

Table 1. Digital brain endocast measures of MCP 3871 PV *Massetognathus ochagaviae* and MCP 1600 PV *Probelesodon kitchingi*. Units = mm, volume units = cm³.

Measure description	<i>M. ochagaviae</i>	<i>P. kitchingi</i>
Total endocast volume	18,926	10,670
Endocast volume excluding the olfactory bulbs cast	18,027	10,055
Total length, measured from the anterior limit of the olfactory bulbs to the foramen magnum	76,56	72,45
Length of the olfactory bulbs cast	29,00	19,00
Length of the telencephalon dorsal surface	22,00	32,00
Length of the cerebellar region (hindbrain), measured from the posterior limit of the hypophyseal cast and the foramen magnum	22,14	13,45
Maximum width, measured on the parafloccular cast region	27,49	21,46
Maximum width of the olfactory bulb casts	10,33	15,66
Maximum width of the telencephalon dorsal surface, measured on the posterior region	14,12	13,42
Maximum height, corresponding to the distance between the ventral limit of the hypophyseal cast and the dorsal surface of the telencephalon		24,17

Table 2. Relative measurements of endocast structures. OB = olfactory bulbs; ROMB = rhombencephalon; TEL = telencephalon; TL = endocast total length; SL = skull length; units = mm.

Specimen	OB	TEL	ROMB	TL	SL
PVL 4016 <i>Massetognathus</i> sp.	24/38%	20/31,74%	19/30,15%	63	95
MCP 3871 PV <i>M. ochagaviae</i>	29/39,72%	22/30,13%	22/30,13%	73	171
PVL 4015 cf. <i>Probelesodon</i>	17/35,41%	20/41,66%	11/22,91%	48	120
MCP 1600 PV <i>P. kitchingi</i>	19/27,14%	32/45,71%	19/27,14%	70	166

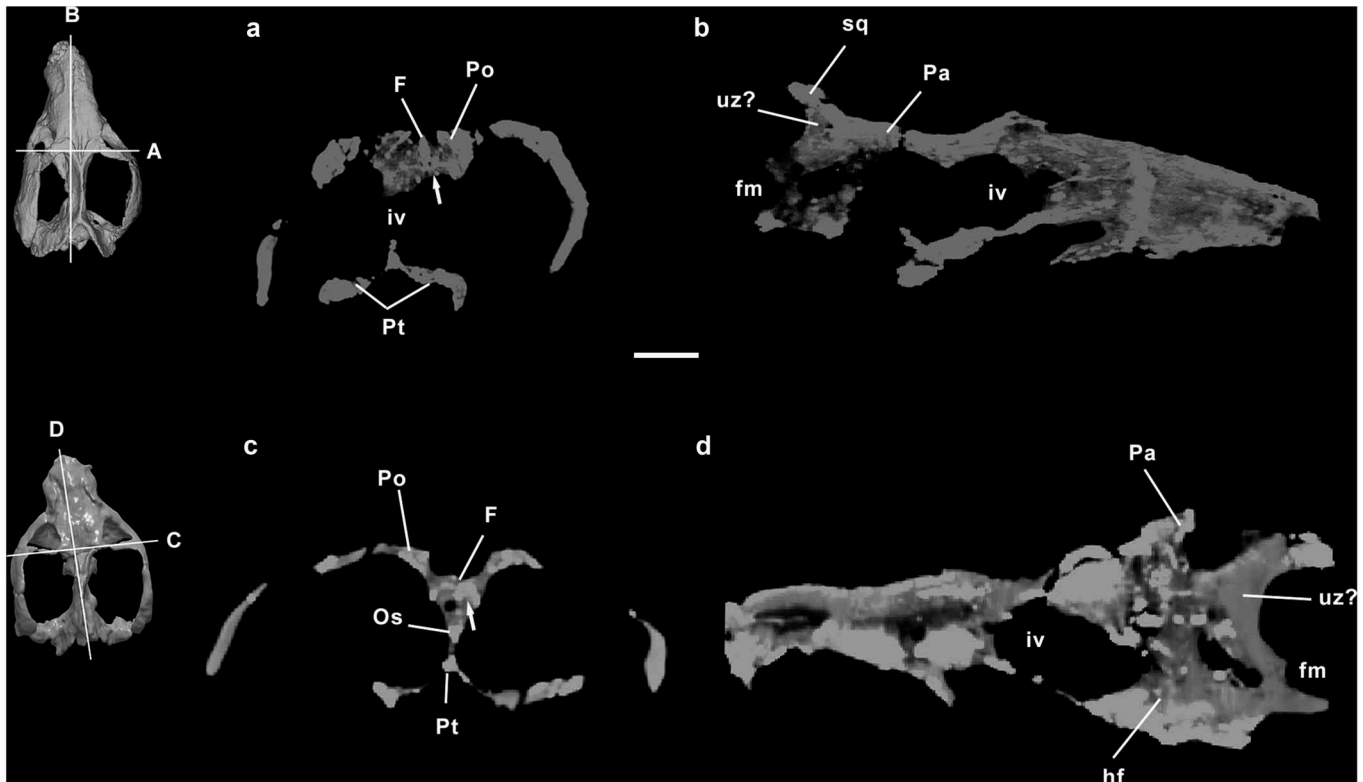


Figure 3. Computed tomography slices of the non-mammaliaform cynodonts studied. (a, b), MCP 1600 PV *Probelesodon kitchingi*. (c, d), MCP 3871 PV *Massetognathus ochagaviae*. The 3D model of the skulls shows the position of the slices. The arrows indicate the internal groove of the frontals, which delimits the olfactory bulbs. Scale bar: 20 mm.

olfactory peduncles; Os, orbitosphenoid; Pa, parietal; pb, pineal body; pfl, parafoveal cast; Po, postorbital; Pt, pterygoid; sq, squamosal; tel, telecephalon; uz, unossified zone.

Results

General aspects

The endocranial casts of MCP 3871 PV *M. ochagaviae* and MCP 1600 PV *P. kitchingi* show a tubular and narrow shape that can be delimited between the foramen magnum and a groove on the internal cavity of the skull. This groove results from an internal thickening of the frontal bones (Figure 3) and can be used to delimit the anterior limits of the olfactory bulb casts. The presence of a broad interorbital vacuity on both species and orbitosphenoid and the presphenoid bones being partially ossified, favours the visualisation of the ventral limits of the anterior region of endocasts (Figure 3). The digital endocasts gradually widen posteriorly, reaching their maximum width at the cerebellar region (27,49 mm and 21,46 mm in *M. ochagaviae* and *P. kitchingi*, respectively; Table 1), as represented by the *parafoveoli* casts. The total length of the digital brain endocasts, measured between the anterior limit of the olfactory bulbs and the foramen magnum is 76,56 mm in *M. ochagaviae* and 72,45 mm in *P. kitchingi* (Table 1) and corresponds to approximately 42% of skull length (171,9 mm and 166,0 mm, respectively) in both species.

The contact between the telencephalon and olfactory bulbs can be delimited by a slope on the endocast ventral region formed by the interorbital vacuity curvature (Figures 4 and 5). On the external surface of the skull, this slope corresponds to the limit between the

parietals and epipterygoid ascending process. Although visible notches of the supraoccipital were not identified, the 'unossified zone' appears to be present in both specimens (Figure 3). Some cranial nerves and possible blood vessels were also identified in both brain endocasts.

Massetognathus ochagaviae endocast

The observable regions of the forebrain in the digital endocast are the olfactory bulbs and telencephalon (cerebral hemispheres). Despite the absence of an ossified cribriform plate, the anterior limit of olfactory bulbs can be delimited in the coronal plane, as previously mentioned. In MCP 3871 PV *M. ochagaviae*, the olfactory bulbs cast extend throughout the frontals, reaching the level of the midpoint of the orbits, and is connected to the telencephalon through peduncles (Figure 4). In the dorsal view, it is long, narrow and widens anteriorly, corresponding to 37,87% (29 mm; Table 2) of the total endocast length. This expansion on the anterior region represents the two olfactory bulbs, from which the longitudinal groove is absent (Figure 4).

The telencephalon is tubular in shape, representing approximately 30% (22 mm; Table 2) of endocast total length, without expansion on the posterior region. The dorsal surface is flat, with no clear evidence of a median sulcus (= longitudinal fissure) dividing the cerebral hemispheres (Figure 4). While present data on *Massetognathus* MCP-3871-PV does not allow the visualisation of a parietal foramen, a pineal body is present (Figure 4). Notably, there is a well-marked hypophyseal cast on the ventral region of the endocast, which fills the *sella turcica* on the basisphenoid/parasphenoid complex (Figure 3).

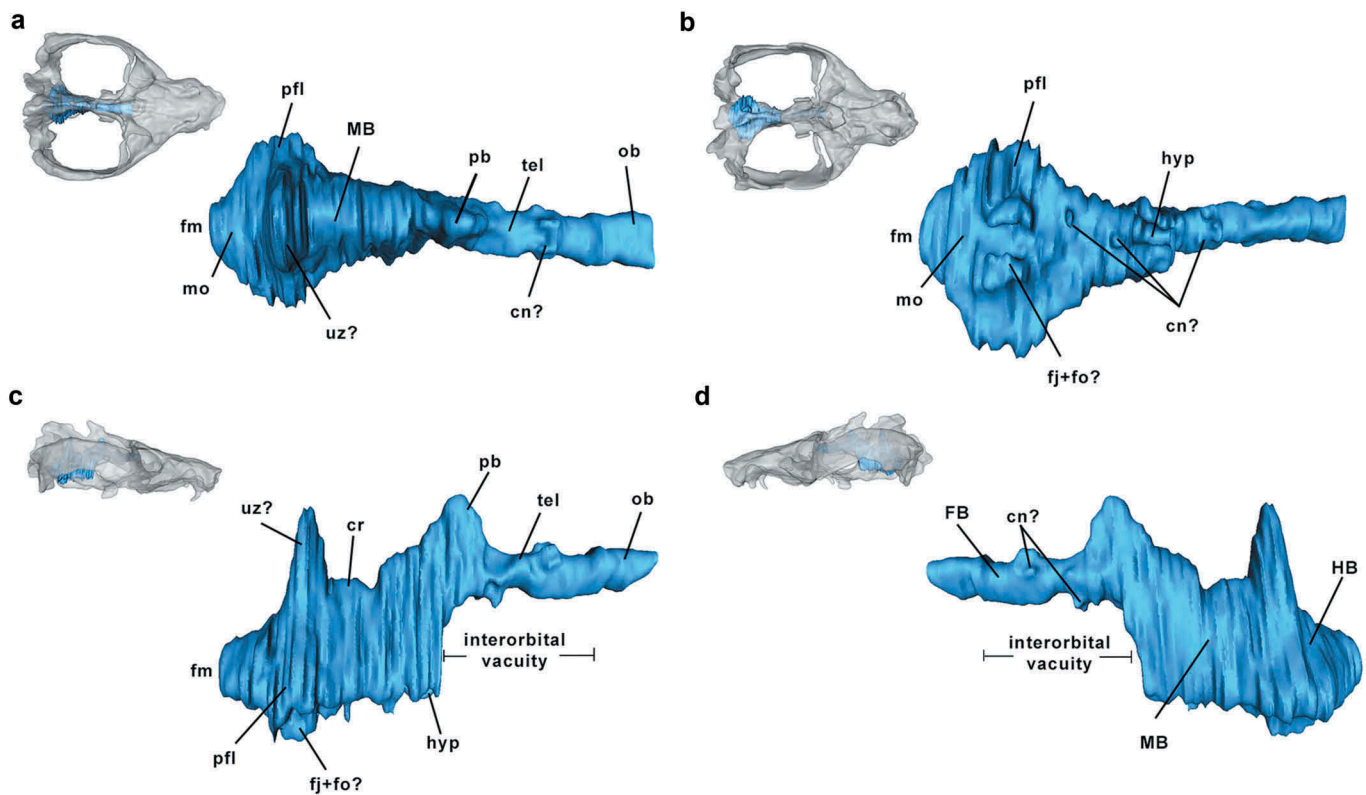


Figure 4. Digital endocast of MCP 3871 PV *Massetognathus ochagaviae* from southern Brazil. (a), dorsal view; (b), ventral view; (c), right lateral and (d), left lateral views. Skulls in transparency show the position of the brain endocast on the brain cavity. Images are not to scale.

In the lateral view, directly after the slope formed on the posterior region of the telencephalon, a prominence is present and can be interpreted as the anterior *colliculi* (Figure 4). Other midbrain structures are also visible in the lateral view.

The hindbrain region is also visible in the lateral view, located posterior to the hypophysis cast. This region is represented by the parafloccular casts, which constitute the widest region of the brain endocast (Figure 4). In MCP 3871 PV *M. ochagaviae*, the *paraflocculi* casts are rounded, laterally directed and prominent in the dorsal view. There is no evidence of any structure that could indicate a division between the cerebellar hemispheres. A clear visualisation of the jugular foramen and fenestra oval casts is impaired due to poor preservation of the basicranium on the posterior region of the basisphenoid. Despite this, it remains possible to observe symmetrical undefined structures that could indicate the jugular foramen and fenestra oval casts (Figure 4).

Although the presence of a supraoccipital notch was not identified in the endocranial cavity, an unossified region filled with hard rock matrix is present (Figure 3). Moreover, some projections were observed on the telencephalic surface: two on the dorsal region, two laterally located and three on the ventral region (Figure 4). These structures could indicate cranial nerves casts or blood vessels.

Probelesodon kitchingi endocast

The olfactory bulbs cast are shorter (19 mm; Table 2) than observed in MCP 3871 PV *M. ochagaviae*, corresponding to 27,14% of the endocast total length and extending almost the entire length of the frontals (Figure 5). However, it widens anteriorly (15,66 mm) and the olfactory bulbs are more developed and expanded laterally (Figure 5). There is a well-defined longitudinal groove between

the bulbs, although they are not clearly separated from each other (Figure 5). In the lateral view, a slope is formed from the posterior region of the olfactory bulbs cast to the anterior portion of the telencephalon (Figure 5). On the external surface of the skull, this slope is represented by the superior region of the interorbital vacuity. Therefore, this narrowing could indicate the presence of peduncles connecting the olfactory bulbs to the telencephalon.

The telencephalon is anteroposteriorly elongated and not posteriorly expanded, corresponding to 45,71% (32 mm; Table 2) of the total endocast length. Since a longitudinal sulcus is absent, the division into two cerebral hemispheres is not present (Figure 5). There is no evidence of a pineal body on the dorsal surface of the endocast and the limits between the brain regions are not well-defined (Figure 5).

The anterior and posterior *colliculi* may not be exposed or preserved in endocasts, as previously mentioned. Nevertheless, on the dorsal surface in the lateral view, there is an inconspicuous prominence posteriorly to the telencephalon slope, which can be interpreted as the collicular region (Figure 5). The digital endocast structure that can be interpreted as the unossified zone is placed more anteriorly, close to the collicular region and forebrain.

Despite the damaged basicranium on the basisphenoid-basioccipital contact, certain cranial nerve casts and foramina were observed. The jugular foramen and the fenestra oval are present and not confluent (Figure 5), with the latter only being visible on the left side of the skull. The hypoglossal nerve cast is located posterior to the jugular foramen. A pair of laterally projected protuberances were observed and indicate the VII cranial nerve casts (Figure 5). The *parafloccular* casts are laterally projected and less prominent than in *M. ochagaviae*. Due to the poor preservation of the basicranium, visualisation of a hypophyseal cast, as

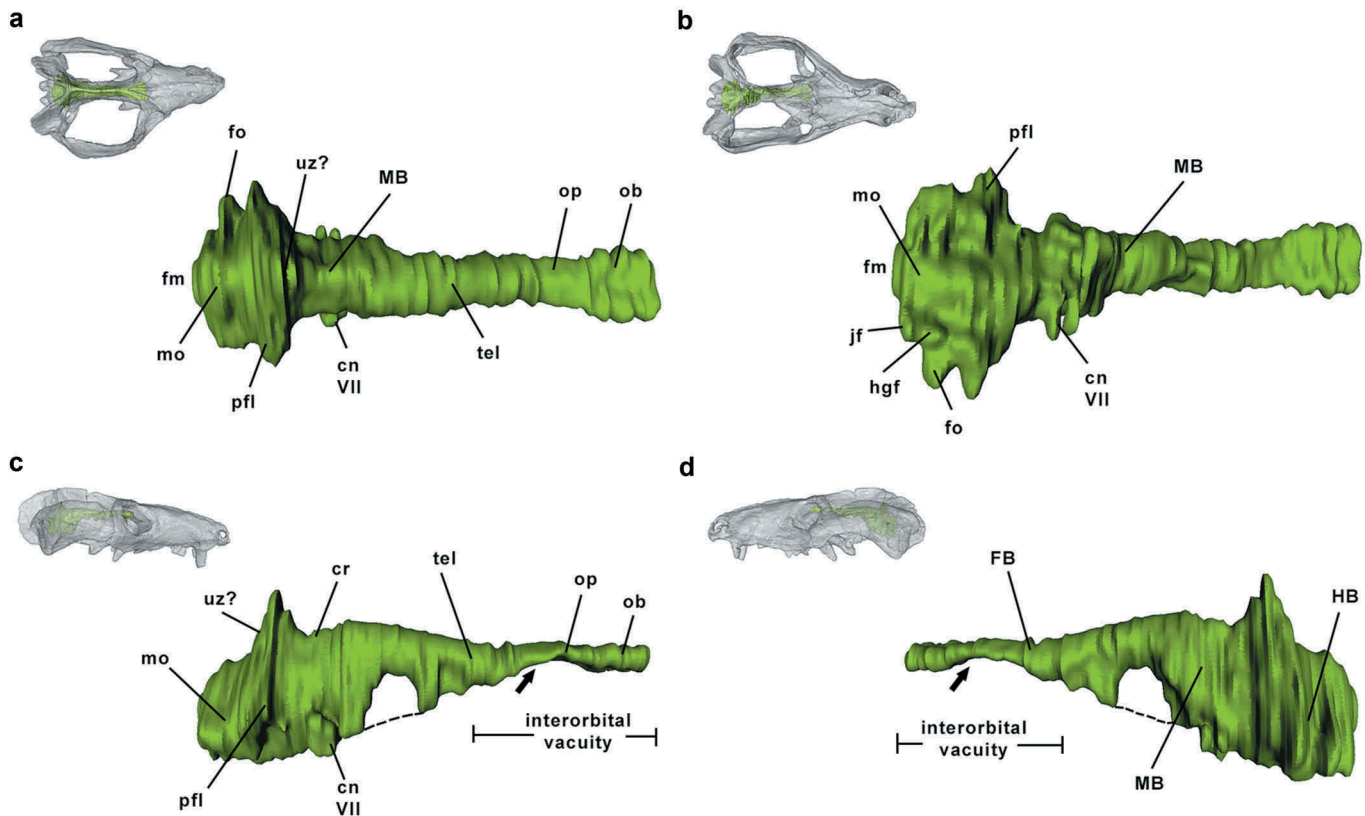


Figure 5. Digital endocast of MCP 1600 PV *Probelesodon kitchingi* from southern Brazil. (a), dorsal view; (b), ventral view; (c), right lateral and (d), left lateral views. Skulls in transparency show the position of the brain endocast on the brain cavity. Arrows indicate the thickening in the olfactory peduncles. Dashed lines represent the ventral limit of the midbrain. Images are not to scale.

vascular impressions and the endocast of the inner ear remain absent.

Encephalisation quotients and relative endocast sizes

The total endocast volumes of *Massetognathus ochagaviae* and *Probelesodon kitchingi* are 18,926 cm³ and 10,670 cm³, respectively (Table 1). To test if the pineal body influenced the total endocast volume obtained for *M. ochagaviae*, we removed the structure, which resulted in a volume of 18,289 cm³ (SI file). Thus, that was not the cause for the high volume observed. Removal of the olfactory bulbs cast volume did not result in significant differences in total endocast volumes (18,027 cm³ and 10,055 cm³ for *M. ochagaviae* and *P. kitchingi*, respectively; Table 1). The skull length of the specimens used in this study is similar (SI file). Consequently, the body masses estimated for both species resulted in approximated values (8,137 g and 13,731 g for *M. ochagaviae*; 7,318 g and 12,350 g for *P. kitchingi*) that were greater than those obtained for *Massetognathus* sp. (1,371 g and 2,359 g) and *Probelesodon* sp. (2,799 g and 4,815 g) by Quiroga (1979, 1980).

According to Quiroga (1980), the EQ values obtained through Equation (1) (see Materials and Methods) for body mass estimation were overestimated. We confirmed these results in the present study, in which EQs calculated with Equation (1) were higher (0,41 and 0,25 for *M. ochagaviae* and *P. kitchingi*, respectively) than the values observed for other non-mammaliaform cynodonts using Jerison's EQ; therefore we used the results from Equation (2) to compare the results of previous works. The EQ values resulting from the Manger (Equation 4) formula were higher than those resulting from Jerison's (Equation 3) EQ (see Table 3). For

comparative purposes and considering that Manger's EQ is more mathematically accurate, all results cited here follow that method.

The EQ calculated for *M. ochagaviae* (0,33) was higher than those resulting from the compared non-mammaliaform cynodonts (Table 3): *Massetognathus* sp. (0,21), *Probelesodon* sp. (0,16), *Exaeretodon* sp. (0,12), *E. riograndensis* (0,26; 0,30), *Siriusgnathus* (0,31), *Probainognathus* (0,18), *Therioherpeton* (0,27) and *Brasilitherium* (0,22); and the same value as *Riograndia* (0,33). The EQ obtained for *P. kitchingi* (0,20) was higher than the calculated for *Probelesodon* sp. and follows the pattern observed for other non-mammaliaform cynodonts, as previously mentioned.

Regarding the relative sizes of MCP 3871 PV *M. ochagaviae* OB (37,87%), T (28,73%) and HB (28,73%) in comparison with PVL 4016 *Massetognathus* sp., the proportions were comparable (38%, 31,74% and 30,15%, respectively). In MCP 1600 PV *P. kitchingi*, the OB is shorter (26,22%) than in PVL 4015 *Probelesodon* sp. (35,41%); however, the T (44,16% and 26,22%) and HB (41,66% and 22,91%) evidence suggests that these components were proportionally longer (Table 2/Figure 6).

Discussion

Analysis of the digital cranial endocasts of *M. ochagaviae* and *P. kitchingi* revealed new features not previously described for these genera. CT-scan images allowed the clear visualisation of a well-defined hypophyseal cast in *M. ochagaviae*, which is not as discernible in the PVL 4016 *Massetognathus* sp. natural endocast (Quiroga 1979). In MCP 1600 PV *P. kitchingi*, the presence of peduncles connecting the olfactory bulbs to the telencephalon highlights a difference between it and the specimen from Argentina.

Table 3. Encephalization Quotients (EQ) calculated to different cynodont taxa. EQ1 = $EV/(0,12BM^{0,66})$, from Jerison (1973); EQ2 = $EV/(0,0535BM^{0,7294})$, from Manger (2006); NA = necessary data to calculations not available; *EQs calculated in this study with available data on the literature. EQ's with two results corresponds to values obtained through Equations (1) and (2) to body mass estimations.

Taxon/specimen	EQ1	EQ2	Source
<i>Thrinaxodon</i>	0,10	NA	Jerison (1973)
<i>Diademodon</i>	0,14	NA	Quiroga (1980)
<i>Massetognathus</i> sp.	0,22;0,15	0,32*;0,21*	Quiroga (1979;1980)
<i>M. ochagaviae</i>	0,41;0,29	0,49;0,33	Present study
<i>Exaeretodon</i> sp.	0,15;0,10	0,18*;0,12*	Quiroga (1980)
<i>E. riograndensis</i> CAPPA 0030	0,39*;0,28*	0,4*;0,30*	Pavanatto et al. (2019)
<i>E. riograndensis</i> CAPPA 0227	0,31*;0,22*	0,38*;0,26*	Pavanatto et al. (2019)
<i>Siriusgnathus</i>	0,4*;0,28*	0,46*;0,31*	Pavanatto et al. (2019)
<i>Probesodon</i> sp.	0,18;0,13	0,24*;0,16*	Quiroga (1979;1980)
<i>P. kitchingi</i>	0,25;0,17	0,30;0,20	Present study
<i>Probainognathus</i>	0,17;0,12	0,26*;0,18*	Quiroga (1980)
<i>Therioherpeton</i>	0,23;0,16	0,40*;0,27*	Quiroga (1984)
<i>Riograndia</i>	0,22	0,33	Rodrigues et al. (2018)
<i>Brasilitherium</i>	0,15	0,22	Rodrigues et al. (2014)
<i>Morganucodon</i>	NA	0,32	Rowe et al. (2011)
<i>Hadrocodium</i>	NA	0,49	Rowe et al. (2011)
<i>Obdurodon</i>	0,78	1,00	Macrini et al. (2006)
<i>Triconodon</i>	NA	0,49	Kielan-Jaworowska (1983)
<i>Chulsanbaatar</i>	NA	0,55	Kielan-Jaworowska (1983)
<i>Kryptobaatar</i>	0,45*;0,32*	0,71	Kielan-Jaworowska and Lancaster (2004)
<i>Ptilodus</i>	NA	0,49	Kielan-Jaworowska (1983)
<i>Vincelestes</i>	0,27	0,37	Macrini et al. (2007)
<i>Kennalestes</i>	NA	0,36	Kielan-Jaworowska (1984)

Digital brain endocasts also facilitated the clear visualisation of the ventral region, including cranial nerve casts and foramina.

According to Quiroga (1979) the midbrain (mentioned by the author as the mesencephalon) was only exposed ventrally, while the cerebellar region was represented by the laterally projected *paraflocculi* casts. Quiroga (1979) described that structure in PVL 4016 *Massetognathus* sp. as being caudally directed (cited as *flocculus* by the author); however, on MCP 3871 PV *M. ochagaviae* *paraflocculi* casts, in the dorsal view, the structure is rounded, laterally directed and prominent. Moreover, we suggest that the anterior *colliculi* (midbrain structure) could be dorsally exposed and represented by prominences on the dorsal surface of the posterior region of the endocast in both species. Therefore, the non-mammaliaforms *Probainognathus* (Quiroga 1980), *P. kitchingi* and *M. ochagaviae* present this midbrain structure as being exposed on the dorsal region of the brain endocast.

Quantitative comparison of the endocast structures of the specimens in the present study against previously described specimens in these genera has raised some questions. Considering the larger skulls of the specimens analysed here, could PVL 4016 *Massetognathus* sp. and PVL 4015 *Probesodon* sp. be considered not fully-grown individuals? Also, can we infer ontogenetic stages from endocast analysis and EQs? In a study of *Massetognathus pascuali* specimens from the Argentinian Chañares Formation, Abdala and Giannini (2000) established an ontogenetic sequence for the species, with the presence and position of the parietal foramen being relevant features considered. According to Abdala and Giannini (2000), the parietal foramen is in the middle of the temporal region in smaller specimens (skull length < 100 mm), while it is vestigial and more anteriorly located in larger specimens, laterally bordered by the enlarged posterior extension of the postorbital. Indeed, in the first description of MCP 3871 PV (Liu et al. 2008), there was no mention of a pineal (= parietal) foramen for *M. ochagaviae*. However, using the CT scanning, it was possible to observe the presence of a pineal tube (= pineal body) on the dorsal surface of the endocast. The pineal body is more posteriorly located on the specimen

PVL 4016 *Massetognathus* sp. (Quiroga 1979) in comparison to MCP 3871 PV *M. ochagaviae* (Figure 6). Based on the new data presented by this study and the ontogenetic sequence proposed by Abdala and Giannini (2000), PVL 4016 *Massetognathus* sp. (skull length = 95 mm) can be considered a juvenile and MCP 3871 PV *M. ochagaviae* (skull length = 170 mm) can be considered as an adult.

However, the EQ values obtained in the present study were higher than those calculated for the specimen used by Quiroga (1979). Since the EQ represents an endocast volume/body mass relation, it is expected that the values obtained for young specimens to be higher than those obtained for adults, as the former exhibits a greater relative brain size in comparison to body size. Nevertheless, we suggest that MCP 3871 PV represents a specimen at an advanced ontogenetic stage for *Massetognathus ochagaviae* while PVL 4016 represents a juvenile of *M. pascuali*. Therefore, the EQ value of the latter species should be even lower than previously calculated, resulting in a considerable EQ variation within the genus. In addition, the observed difference in values can be due to the methods used to analyse the brain endocasts (natural versus digital) and body mass estimations. Furthermore, young individuals should not have BM estimation through the heavy habitus equation, as robustness is only established in later ontogenetic stages. This implies that non-adult cynodonts would have substantially higher EQs than adult individuals. Nevertheless, further studies using specimens of *M. pascuali* are necessary to verify these results.

Notably, an ontogenetic sequence is not available to *Probesodon* sp.; therefore, we can not discuss ontogenetic stages based on morphological evidence. However, the difference in skull length between PVL 4015 and MCP 1600 PV (120 mm and 166 mm, respectively) as well as the difference in EQ values (0,16 and 0,20, respectively) can be used as evidence that the specimens are not from the same species. If both specimens were from the same species, the expected EQ value for PVL 4015 should be higher than the EQ value for MCP 1600 PV. This result contradicts the revision of the genus *Chiniquodon* by Abdala and Giannini (2002). Additionally, the proportions of the endocast structures are different. In PVL 4015, the olfactory bulbs represent 35,41% of total endocast length, while this value for MCP 1600 PV is 26,22%. This could indicate variation within the genus or in chiniquodontids, though this needs to be corroborated by additional specimens.

Regarding the Encephalization Quotient, some aspects deserve discussion. Although EQ is the most common methodological approach for comparing brain size among species of different body masses, it has some constraints when applied in palaeontology. First, the body mass of fossils specimens are estimations, which may be an overestimate or underestimate of the actual value. EVr values for fossil taxa lacking postcranial remains are no better than estimations. The method chosen by the authors also influences EQ calculations. As in most non-mammaliaform cynodonts the skull is the only material available, the more commonly used method involves the equations developed by Quiroga (1979, 1980) based on the skull length/body length relationship in Therapsida. As such, we obtained high EQ values in comparison to other non-mammaliaform cynodonts when Equation (1) ($BM = 1,6S^3$) was used (0,49 and 0,30 for *M. ochagaviae* and *P. kitchingi*, respectively). Equation (2) ($BM = 2,7S^3$) resulted in more reliable values (0,33 and 0,20 for *M. ochagaviae* and *P. kitchingi*, respectively); however, for *M. ochagaviae*, it continues higher than other cynodont taxa. Rodrigues et al. (2018) argued that the overestimated EQ's obtained by Quiroga (1979, 1980) for PVL 4016 *Massetognathus* sp. could be due to inaccuracy in endocast volume measurements (using natural endocast extracted

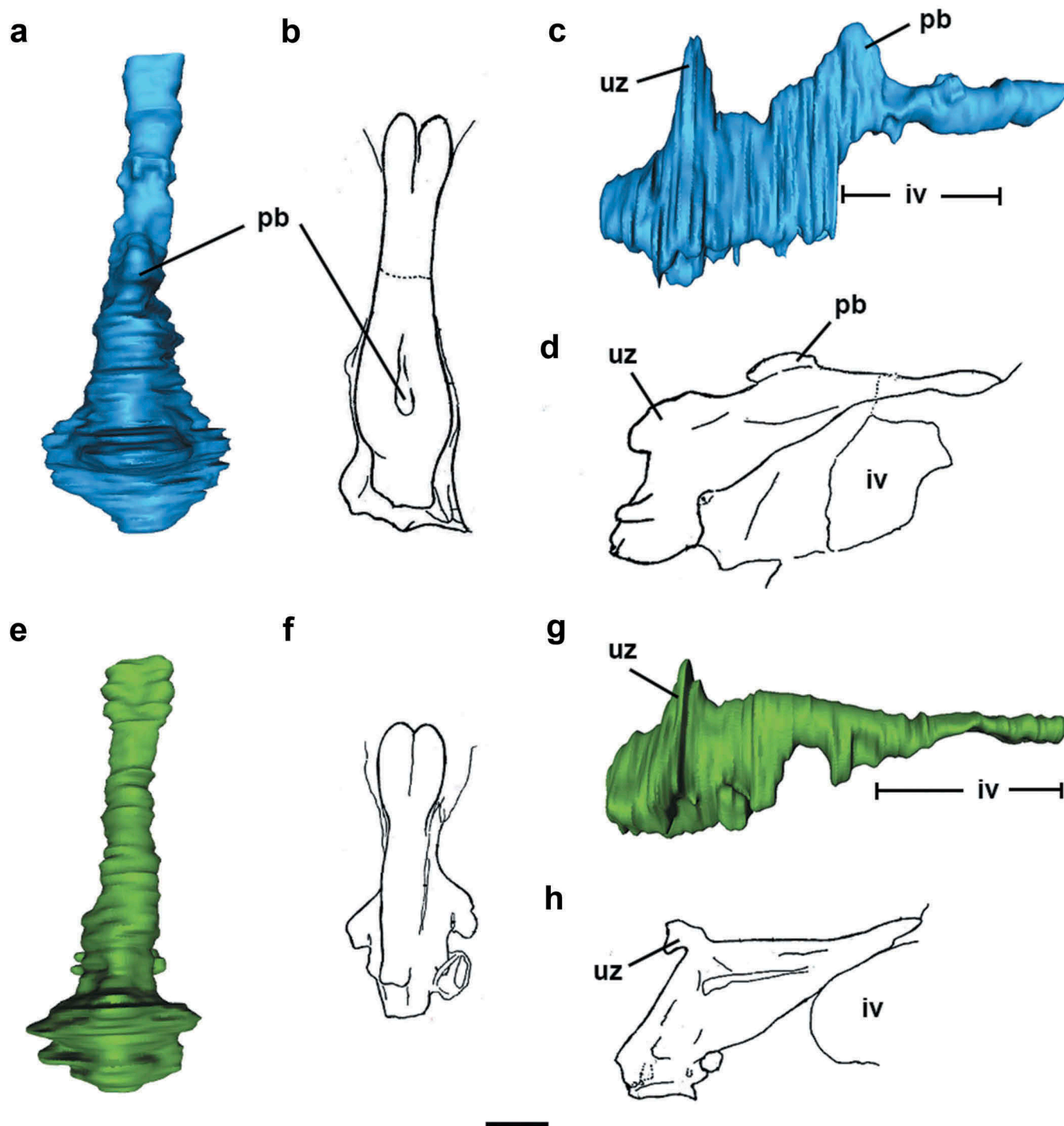


Figure 6. Comparison of the digital endocasts from the present study (digital endocasts) and previous natural endocasts (schematic drawings, modified from Quiroga 1979). (a, c), MCP 3871 PV *M. ochagaviae* in dorsal and lateral views; (b, d), PVL 4016 *Massetognathus* sp.; (e, g), MCP 1600 PV *Probelesodon kitchingi*; (f, h), PVL 4015 cf. *Probelesodon*. Scale bars: approximately 10 mm.

from the skull) or body mass estimation. However, our results suggest that the EQ range (0.22 to 0.15) previously calculated for this genus was not an overestimate. In addition, higher values were obtained to other Cynognathia cynodonts (*E. riograndensis* and *Siriusgnathus*). These results support the alternative hypothesis that increased EQ evolved separately in the sister clades Cynognathia and Probainognathia but discontinued with the extinction of the former group (Rodrigues et al. 2018).

Second, the criterion for the inclusion of olfactory bulb volume in the EQ calculations varies in the literature. Jerison (1973) and Benoit

et al. (2017a, 2017b) excluded the volume of this brain structure, arguing that the braincase in most non-mammalian therapsids is not fully ossified, thus making it difficult to visualise the anterior ventral limit of the endocast. Other authors (e.g. Quiroga 1979, 1980, 1984; Kielan-Jaworowska and Lancaster 2004; Macrini et al. 2006; Rodrigues et al. 2018) provided both calculations. Furthermore, Rodrigues et al. (2014) suggested an initial increase in relative brain size associated with the enlargement of the olfactory bulbs in *Brasilitherium*. In addition, a second pulse of encephalisation was driven by increasing resolution in olfaction and tactile sensitivity and

enhanced neuromuscular coordination in the non-mammalian mammaliaforms *Morganucodon* and *Hadrocodium* (Rowe et al. 2011). Therefore, olfactory enhancement was crucial for the survival of mammaliaforms and basal mammals, as the olfaction is an important sense in extant taxa (Kielan-Jaworowska and Lancaster 2004). Thus, we consider that the exclusion of the olfactory bulb volumes could result in an underestimation of EQ values and a loss of evolutionary information. Therefore, the olfactory bulb volume should be included in the calculations.

Conclusions

We presented endocast analyses of different specimens of the same genera, which facilitated a discussion concerning brain morphology variation within a cynodont family or genus as well as ontogenetic stage inferences. More recently, with the application of non-destructive techniques in palaeontology, such as CT-scan, it is possible to study more than one skull from the same species. Thus, it is relevant to discuss possible intraspecific variation on the endocasts and the ontogeny of fossils. Moreover, CT scans provide a more accurate analysis of the morphology and are more reliable than previous studies using natural endocasts. Despite the problems discussed here regarding the use of Encephalization Quotient in paleoneurological studies, it remains to be the best available method to analyse brain evolution in a variety of vertebrate species. Therefore, it should be interpreted with caution to avoid bias when using extinct taxa.

In addition, recent studies on basal therapsids (Castanhinha et al. 2013; Laaß 2015; Benoit et al. 2017a, 2017b) revealed morphological diversity in neural structure, thus allowing inferences regarding behaviour of these fossil groups. However, our knowledge concerning the brain morphology of more basal synapsids remains scarce, especially for non-mammaliaform cynodonts. The analysis of digital cranial endocasts is important to obtain an improved understanding of how synapsids evolved and thrived as the dominant group during the Permian and survived the extinction event at the end of that period by occupying a variety of niches.

Acknowledgments

The authors are indebted to João Borges and Dario Anschau, from Instituto do Cérebro (InsCer/PUCRS), for providing access to the medical CT-scan and for showing interest on palaeontological research. Vanessa Macedo and Jayme Marques (MCT-PUCRS) provided help with text revision and software use. Drs. Ana Maria Ribeiro (FZB), Cesar L. Schultz (UFRGS) and Julia B. Desojo (MLP) provided helpful comments to the original MSc volume of CAH. We also thank the modifications suggested by the blind reviewers that significantly allowed to improve the quality of this paper. CAH received an MSc scholarship from CNPq (2016–2018), and is currently funded by a CAPES PhD scholarship.

Disclosure statement

No potential conflict of interest was reported by the authors.

Funding

This work was supported by the Conselho Nacional de Desenvolvimento Científico e Tecnológico [830432/1999-0]; Paleontological Society [PalSIRP Sepkoski Grant 2016].

ORCID

Carolina A. Hoffmann  <http://orcid.org/0000-0003-0720-1633>
M. B. Soares  <http://orcid.org/0000-0002-8393-2406>
M. B. de Andrade  <http://orcid.org/0000-0002-3452-801X>

References

- Abdala F, Giannini NP. 2000. Gomphodont cynodonts of the Chañares formation: the analysis of an ontogenetic sequence. *J Vertebr Paleontol.* 20:501–506.
- Abdala F, Giannini NP. 2002. Chiniquodontid cynodonts: systematic and morphometric considerations. *Palaeontology.* 45:1151–1170.
- Abel RL, Laurini CR, Richter M. 2012. A palaeobiologist's guide to 'virtual' micro-CT preparation. *Palaeontol Electron.* 15:1–17.
- Barberena MC. 1981. Uma nova espécie de *Massetognathus* (*Massetognathus ochagaviae*, sp. nov.) da Formação Santa Maria, Triássico do Rio Grande do Sul. [A new species of *Massetognathus* (*Massetognathus ochagaviae*) from Santa Maria Formation, Rio Grande do Sul state Triassic]. *Pesquisas.* 14:181–195. Portuguese.
- Benoit J, Abdala F, Den Brandt MJV, Manger PR, Rubidge BS. 2015. Physiological implications of the abnormal absence of the parietal foramen in a late Permian cynodont (Therapsida). *Sci Nat.* 102. doi:10.1007/s00114-015-1321-4.
- Benoit J, Fernandez V, Manger PR, Rubidge BS. 2017a. Endocranial casts of pre-mammalian therapsids reveal and unexpected neurological diversity at the deep evolutionary root of mammals. *Brain Behav Evol.* doi:10.1159/000481525
- Benoit J, Manger PR, Norton L, Fernandez V, Rubidge BS. 2017b. Synchrotron scanning reveals the palaeoneurology of the head-butting *Moschops capensis* (Therapsida, Dinocephalia). *PeerJ.* doi:10.7717/peerj.3496
- Bonaparte JF. 1966. Sobre las cavidades cerebral, nasal y otras estructuras del craneo de *Exaeretodon* sp. (Cynodontia-Traversodontidae). [About the brain cavity, nasal and other structures of the skull of *Exaeretodon* sp.]. *Acta Geol Lilloana.* 8:5–11. Spanish.
- Bronzati M, Rauhut OWM, Bittencourt JS, Langer MC. 2017. Endocast of the Late Triassic (Carnian) dinosaur *Saturnalia tupiniquim*: implications for the evolution of brain tissue in Sauropodomorpha. *Nat Sci Rep.* doi:10.1038/s41598-017-11737-5
- Butler AN, Hodos W. 2005. Comparative vertebrate neuroanatomy: evolution and adaptation. New Jersey: Wiley.
- Butler E, Abdala F, Botha-Brink J. 2019. Postcranial morphology of the early Triassic epicynodont *Galesaurus planiceps* (Owen) from the Karoo basin, South Africa. *Palaeontology.* 5(1):1–32.
- Castanhinha R, Araújo R, Júnior LC, Angielczyk KD, Martins GG, Martins RMS, Chauiya C, Beckmann F, Wilde F. 2013. Bringing dicynodonts back to life: paleobiology and anatomy of a new Emydopoid genus from the Upper Permian of Mozambique. *PLoS One.* doi:10.1371/journal.pone.0080974
- Cnudde V, Boone MN. 2013. High resolution X-ray computed tomography in geosciences: A review of the current technology and applications. *Earth-Sci Rev.* 123:1–17.
- Cunningham JA, Rahman IA, Lautenschlager S, Rayfield EJ, Donoghue PCJ. 2014. A virtual world of paleontology. *Trends Ecol Evol.* 29:347–357.
- de Oliveira TV, Schultz CL. 2016. Functional morphology and biomechanics of the cynodont *Trucidocynodon riograndensis* from the Triassic of Southern Brazil: pectoral girdle and forelimb. *Acta Palaeontol Pol.* 61:377–386.
- Edinger T. 1964. Midbrain exposure and overlap in mammals. *Am Zool.* 4:5–19.
- Eisenberg JF. 1981. The mammalian radiations: an analysis of trends in evolution, adaptations and behavior. Chicago: University of Chicago Press.
- Hoffmann CA, Andrade MB, Soares MB, Marques JM. 2017. CT scan data collection through low kv protocols provides accurate data on non-mammalian cynodont from the Santa Maria formation, Brazil. Poster presented in: SVP 77th Annual Meeting; Aug 23–26; Calgary, Alberta, Canada.
- Hopson JA. 1979. Paleoneurology. In: Gans C, Northcutt RG, Ulinski P, editors. *Biology of the Reptilia.* Vol. 9. London: Academic Press; Neurology; p. 39–146.
- Horn BLD, Melo TM, Schultz CL, Philipp RP, Kloss HP, Goldberg K. 2014. A new third-order sequence stratigraphic framework applied to the Triassic of the Parana Basin, Rio Grande do Sul, Brazil, based on structural, stratigraphic and paleontological data. *J S Am Earth Sci.* 55:123–132.
- Jerison HJ. 1973. *Evolution of the Brain and Intelligence.* New York: New York Academic Press.
- Jerison HJ. 1985. Animal intelligence as encephalization. *Philos Trans R Soc Lon B Biol Sci.* 308:21–35.
- Kemp TS. 1979. The primitive cynodont *Procynosuchus*: structure, function, and evolution of the postcranial skeleton. *Philos Trans R Soc Lon B Biol Sci.* 288:217–258.
- Kemp TS. 2009. The endocranial cavity of a nonmammalian eucynodont, *Chiniquodon theotenicus*, and its implications for the origin of the mammalian brain. *J Vertebr Paleontol.* 29:1188–1198.
- Kielan-Jaworowska Z. 1983. Multituberculate endocranial casts. *Palaeovertebrata.* 13:1–12.

- Kielan-Jaworowska Z. 1984. Evolution of the therian mammals in the late Cretaceous of Asia, Part VI, Endocranial casts of eutherian mammals. *Acta Palaeontol Pol.* 46:157–171.
- Kielan-Jaworowska Z, Cifelli RL, Luo Z-X. 2004. Mammals from the age of dinosaurs: origin, evolution and structure. New York: Columbia University Press.
- Kielan-Jaworowska Z, Lancaster TE. 2004. A new reconstruction of multituberculate endocranial casts and encephalization quotient of *Kryptobaatar*. *Acta Palaeontol Pol.* 49:177–188.
- Laaß M. 2015. Virtual reconstruction and description of the cranial endocast of *Pristerodon mackayi* (Therapsida, Anomodontia). *J Morphol.* 276:1089–1099.
- Laaß M, Schillinger B, Kaestner A. 2017. What did the “Unossified Zone” of the non-mammalian therapsid braincase house? *J Morphol.* doi:10.1002/jmor.20583
- Lebrun R. 2018, 07 MorphoDig, an open-source 3D freeware dedicated to biology. IPC5, Paris, France.
- Liu J, Soares MB, Reichel M. 2008. *Massetognathus* (Cynodontia, Traversodontidae) from the Santa Maria formation of Brazil. *Rev Bra Paleontol.* 11:27–36.
- Macrini TE, Rougier GW, Rowe T. 2007. Description of a cranial endocast from the fossil mammal *Vincelestes neuquenianus* (Theriiiformes) and its relevance to the evolution of endocranial characters in Therians. *Anat Rec.* 290:875–892.
- Macrini TE, Rowe T, Archer M. 2006. Description of a cranial endocast from a fossil platypus, *Obdurodon dicksoni* (Monotremata, Ornithorhynchidae), and the relevance of endocranial characters to monotreme monophyly. *J Morphol.* 267:1000–1015.
- Manger PR. 2006. An examination of cetacean brain structure with a novel hypothesis correlating thermogenesis to the evolution of a big brain. *Biol Ver.* doi:10.1017/S1464793106007019.
- Marsicano CA, Irmis RB, Mancuso AC, Mundil R, Chemale F. 2016. The precise temporal calibration of dinosaur origins. *PNAS.* 113:509–513.
- Martinelli AG, Kammerer CF, Melo MP, Neto VDP, Ribeiro AM, Da-Rosa AAS, Schultz CL, Soares MB. 2017. The African cynodont *Aleodon* (Cynodontia, Probainognathia) in the Triassic of southern Brazil and its biostratigraphic significance. *PLoS One.* 12:1–54.
- Napoli JG, Williamson TE, Shelley SL, Brusatte SL. 2017. A digital endocranial cast of the early paleocene (Puercan) ‘archaic’ mammal *Onychodectes tisonensis* (Eutheria: Taeniodonta). *J Mamm Evo.* 25:179–195.
- Pavanatto AEB, Kerber L, Dias-da-Silva S. 2019. Virtual reconstruction of cranial endocasts of traversodontid cynodonts (Eucynodontia: Gomphodontia) from the upper Triassic of Southern Brazil. *J Morphol.* 280:1267–1281.
- Pierini C, Mizusakia AMP, Scherera CMS, Alves DB. 2002. Integrated stratigraphic and geochemical study of the Santa Maria and Caturrita formations (Triassic of the Paraná Basin), southern Brazil. *J S Am Earth Sci.* 15:669–681.
- Quiroga JC. 1979. The brain of two mammal-like reptiles (Cynodontia – Therapsida). *J Hirnforsch.* 20:341–350.
- Quiroga JC. 1980. The brain of the mammal-like reptile *Probainognathus jenseni* (Therapsida, Cynodontia), a correlative paleo-neurological approach to the neocortex at the reptile-mammal transition. *J Hirnforsch.* 21:299–336.
- Quiroga JC. 1984. The endocranial cast of the advanced mammal-like reptile *Therioherpeton cargnini* (Cynodontia – Therapsida) from the middle Triassic of Brazil. *J Hirnforsch.* 25:285–290.
- Rodrigues PG, Martinelli AG, Schultz CL, Corfe IJ, Gill PG, Soares MB, Rayfield EJ. 2018. Digital cranial endocast of *Riograndia guaibensis* (Late Triassic, Brazil) sheds light on the evolution of the brain in non-mammalian cynodonts. *Hist Biol.* doi:doi:10.1080/08912963.2018.1427742
- Rodrigues PG, Ruf I, Schultz CL. 2014. Study of a digital cranial endocast of the non-mammaliaform cynodont *Brasilitherium riograndensis* (Late Triassic, Brazil) and its relevance to the evolution of the mammalian brain. *Paläontol Z.* 88:329–352.
- Rowe TB, Carlson WD, Böttorff WW. 1994. *Trinaxodon*: digital atlas of the skull, CD-ROM (Second Edition for Windows and Macintosh platforms. Austin (TX): University of Texas Press.
- Rowe TB, Macrini TE, Luo Z-X. 2011. Fossil evidence on origin of the mammalian brain. *Science.* 332:955–957.
- Sá-Teixeira AM. 1982. Um novo cinodonte carnívoro (*Probelesodon kitchingi* sp. nov.) do Triássico do Rio Grande do Sul, Brasil. [A new carnivore cynodont (*Probelesodon kitchingi*) from the Triassic of Rio Grande do Sul state, Brazil]. *Comunicações Do Museu De Ciências Da PUCRGS.* 24:1–31. Portuguese.
- Scherer CMS. 2000. Eolian dunes of the Botucatu Formation (Cretaceous) in southernmost Brazil: morphology and origin. *Sediment Geol.* 137:63–84.
- Soares MB, Schultz CL, Horn BLD. 2011. New information on *Riograndia guaibensis* Bonaparte, Ferigolo & Ribeiro, 2001 (Eucynodontia, Trithelodontidae) from the Late Triassic of Southern Brazil: anatomical and biostratigraphic implications. *An Acad Bra Ciênc.* 83:329–354.
- Tafforeau P, Boistel R, Boller E, Bravin A, Brunet M, Chaimanee Y, Cloetens P, Feist M, Hosszowska J, Jaeger JJ, et al. 2006. Applications of X-ray synchrotron microtomography for non-destructive 3D studies of paleontological specimens. *Appl Phys A.* 83:195–202.
- Watson DMS. 1913. Further notes on the skull, brain, and organs of special sense of *Diademodon*. *J Nat Hist.* 12:217–228.
- Zerfass H, Lavina EL, Schultz CL, Garcia AJV, Faccini UF, Chemale F Jr. 2003. Sequence stratigraphy of continental Triassic strata of southernmost Brazil: a contribution to Southwestern Gondwana palaeogeography and palaeoclimate. *Sediment Geol.* 161:85–105.